Research Square

Preprints are preliminary reports that have not undergone peer review.
They should not be considered conclusive, used to inform clinical practice,
or referenced by the media as validated information.

# Chitosan-Intercalated FePS3 as Novel and Efficient Adsorbent for Congo-Red Dye Removal from Aqueous Solution

**O. I. El-Shafey**
National Research Centre
**Shaymaa E. El-shafey**
s_shafey@yahoo.com
National Research Centre
**Amal M. Abdel-karim**
National Research Centre
**Amin A. El-Meligi**
National Research Centre

**Article**

**Keywords:** FePS3, Intercalation, Chitosan, Dye adsorption, Surface area, porosity analysis

**Posted Date:** August 5th, 2026

**DOI:** https://doi.org/10.21203/rs.3.rs-10413324/v1

**License:** This work is licensed under a Creative Commons Attribution 4.0 International License.
Read Full License

**Additional Declarations:** No competing interests reported.

**Version of Record:** A version of this preprint was published at Scientific Reports on November 16th, 2026. See the published version at https://doi.org/10.1038/s41598-026-75300-x.

# Chitosan-Intercalated $FePS_3$ as Novel and Efficient Adsorbent for Congo-Red Dye Removal from Aqueous Solution

**O. I. El-Shafey, Shaymaa E. El-shafey*, Amal M. Abdel-karim, Amin A. El-Meligi**

*Physical Chemistry Department, National Research Centre, 33 El Bohouth St. Dokki, P.O.12622, Giza, Egypt*

*Corresponding authors: **Shaymaa E. El-shafey**

E mail: s_shafey@yahoo.com

## Abstract

This study investigates surface adsorption of Congo red dye (CR) by iron phosphorus trisulphide ($FePS_3$) before and after chitosan (CS) intercalation. The novel intercalation of the chitosan into the layered nanomaterial $FePS_3$ was processed to obtain $FePS_3$-CS. The materials of $FePS_3$ and $FePS_3$-CS were characterized by XRD, FTIR, SEM-EDX, and BET techniques. These tests verified the effective intercalation of the chitosan into the layered nanomaterial $FePS_3$ with improved characteristics for applications involving adsorption. XRD measurements show a slight shift and partial intercalation of CS into $FePS_3$ layers, and some diffraction peaks have disappeared. This behavior may be due to CS as a polymer interacts with $FePS_3$ through electrostatic interactions between the amino/hydroxyl groups of CS and S-containing $FePS_3$ surfaces, and hydrogen bonding. IR and SEM-EDX confirm the presence of CS functional groups and main elements after intercalation with $FePS_3$. $FePS_3$ and $FePS_3$-CS exhibited notable removal of Congo-Red from artificial aqueous solutions. The best adsorption circumstances of $FePS_3$ and $FePS_3$-CS were found to be dye concentration of 50 mg/L, dose of (0.05g and 0.025 g), pH 5, 6, respectively, and a contact time of 90 min. Under these circumstances, the maximum adsorption efficiencies of $FePS_3$ and $FePS_3$-CS are 91.4 and 99%, respectively. According to kinetic study results, a pseudo-second-order kinetic model described the adsorption process, with a high degree of agreement between the experimental data and the model. Moreover, the Freundlich isotherm model provided the best description of equilibrium data, demonstrating multilayer adsorption. These

findings highlight the excellent effectiveness and promise of $FePS_3$ and $FePS_3$-CS as novel adsorbents for dye removal applications.

*Keywords:* $FePS_3$, Intercalation, Chitosan, Dye adsorption, Surface area, porosity analysis

## 1. Introduction

Environmental pollution has exerted severe effects on earth, and it includes various types of pollution, such as air pollution, water pollution, soil pollution, etc.[1-3]. Water pollution is one of the most important types of environmental pollution because it causes severe threats to the environmental ecosystems and human health[4]. Synthetic dyes applied in various industries, for example, textiles, papers, and plastics, could escape into water, causing severe effects because of their potential toxicity and persistent nature [3, 5]. As is reported, synthetic dyes are the backbone of dyeing industries and are expanding globally, reaching about 8 × 105 tons of synthetic dyes produced per year [6, 7].

The layered two-dimensional materials (2D) named transition metal phosphorus trichalcogenides ($MPX_3$, M = Ti, V, Mn, Fe, Ni; X = S or Se) have interesting electronic, magnetic, and optical properties [8, 9]. These properties make them promising 2D layered materials for applications in energy storage, catalysis and surface adsorption, and environmental remediation [10, 11]. The candidate iron phosphorus trisulfide ($FePS_3$) has significantly attracted attention due to its intrinsic magnetic properties, especially antiferromagnetic behavior, wide optical band gap (~1.6–1.8 eV), and the unique layered structure [12-14]. The layered materials could be modified by intercalating organic and polymer compounds [15, 16] . Accordingly, enhancing surface functionality, chemical stability, and adsorption performance could be attained by the intercalation of polymers and organic molecules into the $FePS_3$ layers [17, 18].

Chitosan (CS) is a natural product of polysaccharide and it is produced by deacetylation of chitin. CS is well known for its biodegradability, biocompatibility, non toxic, porous structure, large surface area, and abundance of surface functional groups. It has found

extensive use in medical and industrial fields. It is used as adsorbent due to its distinctive chemical composition. The abundance of amino group (-$NH_2$) and hydroxyl group (-OH) enable it to interact efficiency with a wide range of metal ions, dyes and organic compounds through chelation and hydrogen bonding. Its properties can be improved through chemical modification with groups as thiourea and carboxymethyl; also these groups can coordinate with transition metals in $MPX_3$ and can form hydrogen bond with organic compounds [19, 20].

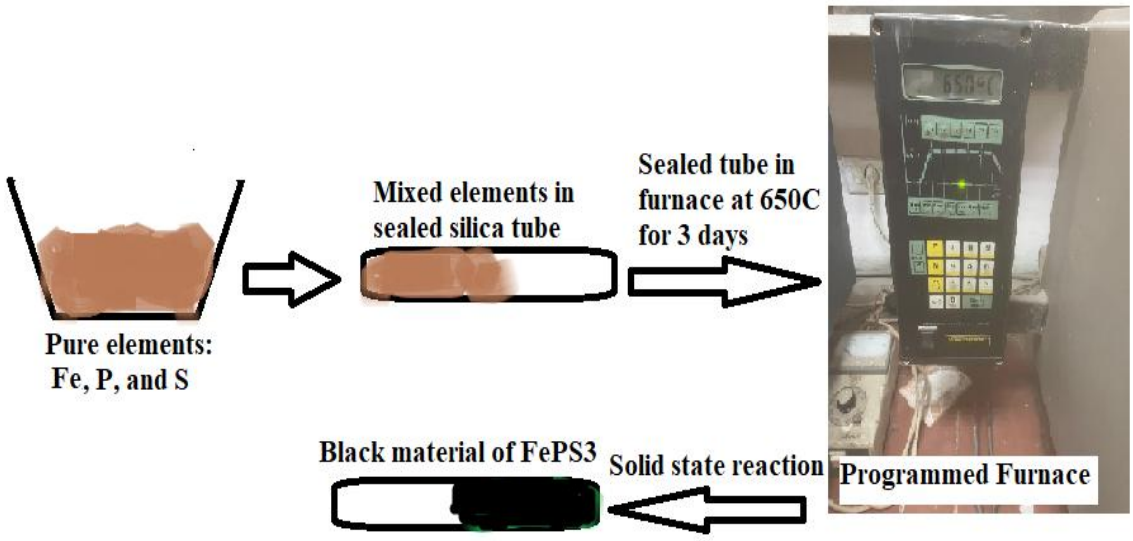
In case of intercalation with $FePS_3$, CS can improve the stability and dispersibility of the layered material in aqueous solutions. In addition, it can introduce additional active adsorption sites for impurities and pollutants. The intercalate compound of $FePS_3$-CS can form a promising composite for dye adsorption and wastewater treatment. This type of treatment for organic dyes, such as methylene blue, methyl orange, and rhodamine B, can help to get rid of these organic hazards, which pollute the environment because of their toxicity and persistence. The electrostatic interactions, hydrogen bonding, π–π stacking, and coordination with surface metal sites are the possible ways of dyes adsorption on 2D materials [21]. For example, Congo red ($C_{52}H_{22}N_6O_6S_2Na_2$) contains active centers including sulfonate groups (–$SO_3^{2-}$), azo linkages (–N=N–), amino group (-$NH_2$) and extended aromatic systems that provide multiple binding modes with adsorbent surfaces [22-25]. The $FePS_3$ structure consists of van der Waals-stacked layers, where Fe atoms are coordinated by S atoms in a distorted octahedral environment, and $P_2S_6^{4-}$ units are incorporated within the lattice [12]. The unique structure of $FePS_3$ supports potential interactions with Congo red through electrostatic attraction between $SO_3^-$of the dye and ferrous ions ($Fe^{2+}$) sites, especially at defect or edge sites. The reason for using Congo red is widely applied in textile industries for dyeing purposes, and has a bright color, high solubility, and stability under various conditions, which contribute to its persistence in the environment [26-28] .

Accordingly, the aim of this study is to investigate the adsorption of dye on $FePS_3$-CS composite as a novel strategy for sustainable water purification technologies.

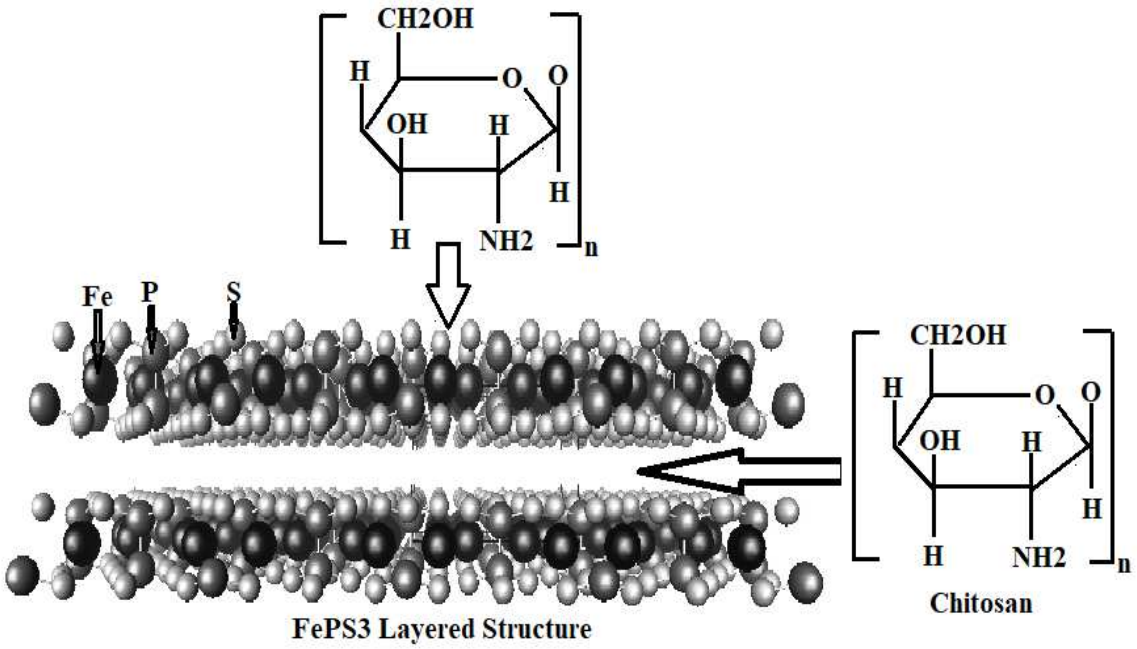
## 2. Experimental Methods

### 2.1. Synthesis of $FePS_3$ and Intercalation with CS

The $FePS_3$ compound was synthesized using a controlled solid-state reaction in a programmed furnace. Stoichiometric amounts of Fe, P, and S powders were thoroughly mixed, sealed in an evacuated silica tube, and heated up to 650 for 3 days, as shown in scheme 1. Intercalation of $FePS_3$ with CS was experimentally processed using wet-chemical method in which 10 ml of CS solution was added to 0.15 g of $FePS_3$ black powder and stirred for 10 hrs at 60 $^oC$. After stirring, the materials were filtered and dried to run the experiments. CS is a linear polysaccharide and has the chemical name (1, 4)-2-amino-2-deoxy-d-glucose. The schematic diagram 2 shows the proposed intercalation of $FePS_3$ with CS.




Scheme 1: Synthesis process of $FePS_3$ layered crystalline material.




Scheme 2: Proposed diagram for intercalation of $FePS_3$ with chitosan (CS). $FePS_3$ was built using Atoms program [29].

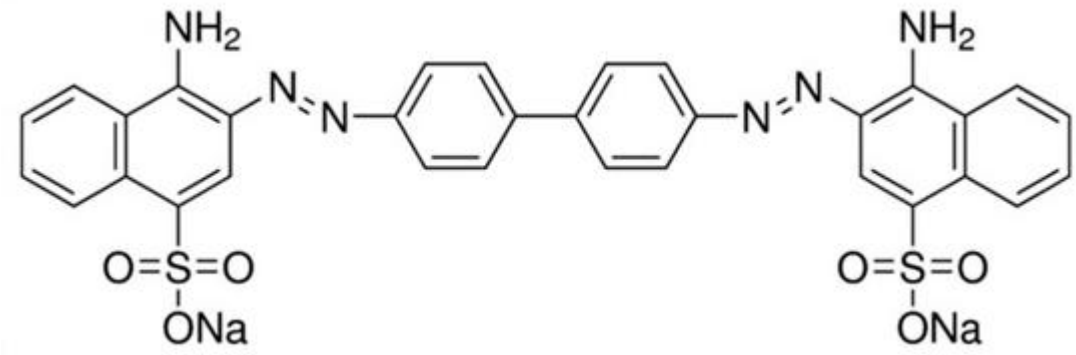
### 2.2. Materials Characterization

XRD was measured using the Bruker D8-Advance diffractometer equipped with Cu kα radiation (λ=0.15418 nm). Fourier transform infrared (FTIR) spectra were recorded using Bruker VERTEX 80 spectrometer coupled with a Platinum Diamond ATR comprises a diamond disk as that of an internal reflector, in the range 4000–400 $cm^{-1}$ with resolution 4 $cm^{-1}$. The surface morphology and elemental composition of the samples were examined using a Quanta FEG 250 scanning electron microscope (SEM) equipped with an energy dispersive X-ray (EDX) detector.

The textural parameters such as Brunauer-Emmett-Teller surface area (SBET, $m^2/g$), total pore volume (VP, $cm^3/g$), mean pore diameter (RP, A) and pore width (WP, nm), were determined by nitrogen adsorption –desorption nalysis at -196 °C using BEL-Sorp analyzer (microtracBEL Crop., Japan).

## 2.3. Adsorption methodology

Congo red dye (CR) is a symmetrical, disulfonated azo dye with a sodium salt forms with molecular from $C_{32}H_{22}N_6O_6S_2Na_2$, and it consists of a biphenyl group connecting two 4-aminonaphthalene-1-sulfonate groups. The chemical structure is shown below, scheme 2:




Scheme 3: Chemical structure of Congo-Red Dye.

The adsorption methodology included preparing a stock solution of Congo red dye (CR, 25 mg/L). The adsorption behavior of dye by the as-prepared adsorbents was tested in a static adsorption mode under different conditions. About 0.025 g of the prepared samples were conducted with 25 mL of CR dye (C0=0.025-50 mg/L) at 25 $^{o}$C under shaking at 220 rpm for 24h to reach equilibrium. The pH was adjusted using either 0.1 M solution of NaOH or HCl.

## 2.4. Adsorption studies

A stock solution of Congo red dye (CR, 25 mg/L) was prepared. The adsorption behavior of dye by the as-prepared adsorbents was tested in a static adsorption mode under different conditions. About 0.025 g of the prepared samples were conducted with 25 mL of CR dye ($C_0$=0.025-50 mg/L) at 25$^{o}$C under shaking at 220 rpm for 24h to reach equilibrium. The pH was adjusted using either 0.1 M solution of NaOH or HCl.

Absorbance readings of remaining CR dye in the prepared solutions have been recorded at triplicate, and the relative standard deviation was < 3%. The experimental data were fitted for linear kinetics and isotherm models with Origin Pro 2016 Version 8. One of the most often measured parameters for evaluating the performance of the applied models is the correlation coefficient ($R^2$) detecting the best experimental data with values greater than 0.95.

The maximum absorbance of the CR dye -supernatant solution was analyzed employing a UV-visible spectrophotometer (Type UV-2401PC) in a 1 cm quartz cuvette to check the characteristic absorption peaks of dye at a wavelength of 490 nm. The removal percentage (% R) of CR dye using samples was amounted by the following equation:

$$\text{R}\,\% = \frac{(C_0 - C_e)\ 100}{C_0} \qquad (1)$$

The amount of CR adsorbed by the solid sample ($q_e$, mg/g) was obtained using this equation:

$$q_e = \frac{(C_0 - C_e)\,V}{m} \qquad (2)$$

Where $C_o$ and $C_e$ (mg/L) is the concentration before and after adsorption , V (L) is the volume of the dye solution, and m (g) is the weight of the $FePS_3$-CS.

### *2.4.1. Adsorption models*

To investigate the adsorption mechanism of Congo red dye onto adsorbent, three common kinetic models were applied. First model was the Lagergren-first-order kinetic model (quation3) [30] [31] :

$$log\ (q_e - q_t) = log\ q_e - \frac{k_1 t}{2.303} \qquad (3)$$

While pseudo-second-order kinetic model which is expressed by the equation (4)[30]

$$\frac{t}{q_t} = \frac{1}{k_2 q_e^{\,2}} + \frac{t}{q_e} \qquad (4)$$

In the adsorption process, *qt* (mg/g) represents the amount of CR adsorbed by the adsorbent at specific time *t* (min), while *qe* (mg/g) is the adsorption capacity at equilibrium. The pseudo-first order rate constant, $k_1$ ($min^{-1}$) was calculated from the slope of the plot of log (qe–qt) versus t , as described by equation (2). The pseudo-second-order rate constant, $k_2$ (g $mg^{-1}min^{-1}$), was calculated from the slope$1/q_e$ and the intercept$1/k_2qe^2$ of the linear plots $t/q_t$ against t, equation (4).

The intra-particle diffusion model as proposed by Weber and Morris [32] is described by the equation (5):

$$q_t = k_{id}\, t^{1/2} + C \qquad (5)$$

Where $k_{id}$ (mg/g $min^{1/2}$) is the intra-particle diffusion rate constant and C (mg/g) is the intercept, which can be calculated from the linear plots of $q_t$ versus $t^{1/2}$.

### *2.4.2. Adsorption isotherm studies*

The equilibrium adsorption behavior of CR dye onto the prepared adsorbents was evaluated using Langmuir, Freundlich, adsorption isotherms to better understand the adsorption mechanism [33, 34]. These models were fitted to the experimental equilibrium data and their linear forms of these isotherms are given in the following equations:

*Langmuir equation*

$$C_e / q_e = \frac{1}{K_L Q_m} + \frac{1}{Q_m} C_e \qquad (6)$$

Where $C_e$ (mg/L) is the equilibrium concentration of adsorbate in solution, $q_e$ (mg/g) is the amount of CR dye adsorbed at equilibrium , and $Q_m$ (mg/g) is the monolayer adsorption capacity, and $K_l$ (L /mg) is the Langmuir adsorption constant , which is

related to the free energy of adsorption according to ($K_L$ α $e^{-\Delta G/RT}$). The standard Gibbs free energy of adsorption, ΔG (kJ/mol) was calculated using $\Delta G = - RT \ln K_s$.

Where R is the universal gas constant, T is absolute temperature, and $K_s$ is the adsorption equilibrium constant.

The values of $q_t$ and $K_L$ were obtained from the slope and intercept of the linear Langmuir isotherm plot $C_e/q_e$ vs. $C_e$.

*Freundlich isotherm*

The adsorption equilibrium was analyzed using Freundlich isotherm model, whose linear form is given in equation [34]

$$\log q_e = \log K_F + \frac{1}{n} \log C_e \quad (7)$$

Where $K_F$ (mg/g $(L/mg)^{1/n}$) is Freundlich constant related to adsorption capacity, while 1/n is the adsorption intensity. The value of $K_F$ and 1/n were determined from the intercept and slope of the linear plot *log* $q_e$ against *log* $C_e$, respectively.

To justify the applicability of each adsorption isotherm model was evaluated the correlation coefficient ($R^2$), with the model exhibiting the highest $R^2$ value considered to provide the best description of the experimental behavior

## 3. Results and Discussion

### 3.1 XRD of $FePS_3$ and $FePS_3$-CS

The XRD pattern of $FePS_3$ shows typical hkl phases, as presented in Figure 1a, and it is indexed as a monoclinic crystal structure with a space group of 2C/m[35-37]. The intercalation of $FePS_3$ with CS has processed under stirring for 10 hours at 60 $^oC$. The presence of van der Waals gaps between the $FePS_3$ layers facilitates the intercalation of various compounds and ions which could change the crystal structure from monoclinic to trigonal structure and the space group could change from C2/m to R3m due to intercalation of organic compound [38].

Accordingly, the hkl phases of $FePS_3$ have changed after intercalation or have shifted or have disappeared. As observed, the XRD of $FePS_3$-CS shows slight shifting of some hkl phases and disappearing of others, as shown in Figure 1b. The presence of phases at 28.2° and 33.2° suggests the partial intercalation of CS within the $FePS_3$ galleries and the formation of new structural ordering. The absences of significant expansion of the hkl phase (001) imply limited d-spacing expansion and predominantly surface/interface interactions[17, 38] . In addition, the slight shift of the hkl phase (001) after CS intercalation, together with preservation of the characteristic $FePS_3$ XRD peaks, indicates that the layered crystal framework of $FePS_3$ remains intact. Also, the absence of a notable low-angle shift suggests that CS does not induce major expansion of the $FePS_3$ layers, implying predominantly partial intercalation and surface adsorption of CS. The aforementioned behavior of CS intercalation into $FePS_3$ layers is attributed to hydrogen bonding and electrostatic interactions between the amino/hydroxyl groups of CS and sulfur-containing $FePS_3$ surfaces; this is consistent with previous studies on polymer–layered material composites, as well as the steric hindrance of large biopolymers, such as CS, limits the possibility of full intercalation into 2D layered materials[12, 19, 39] .

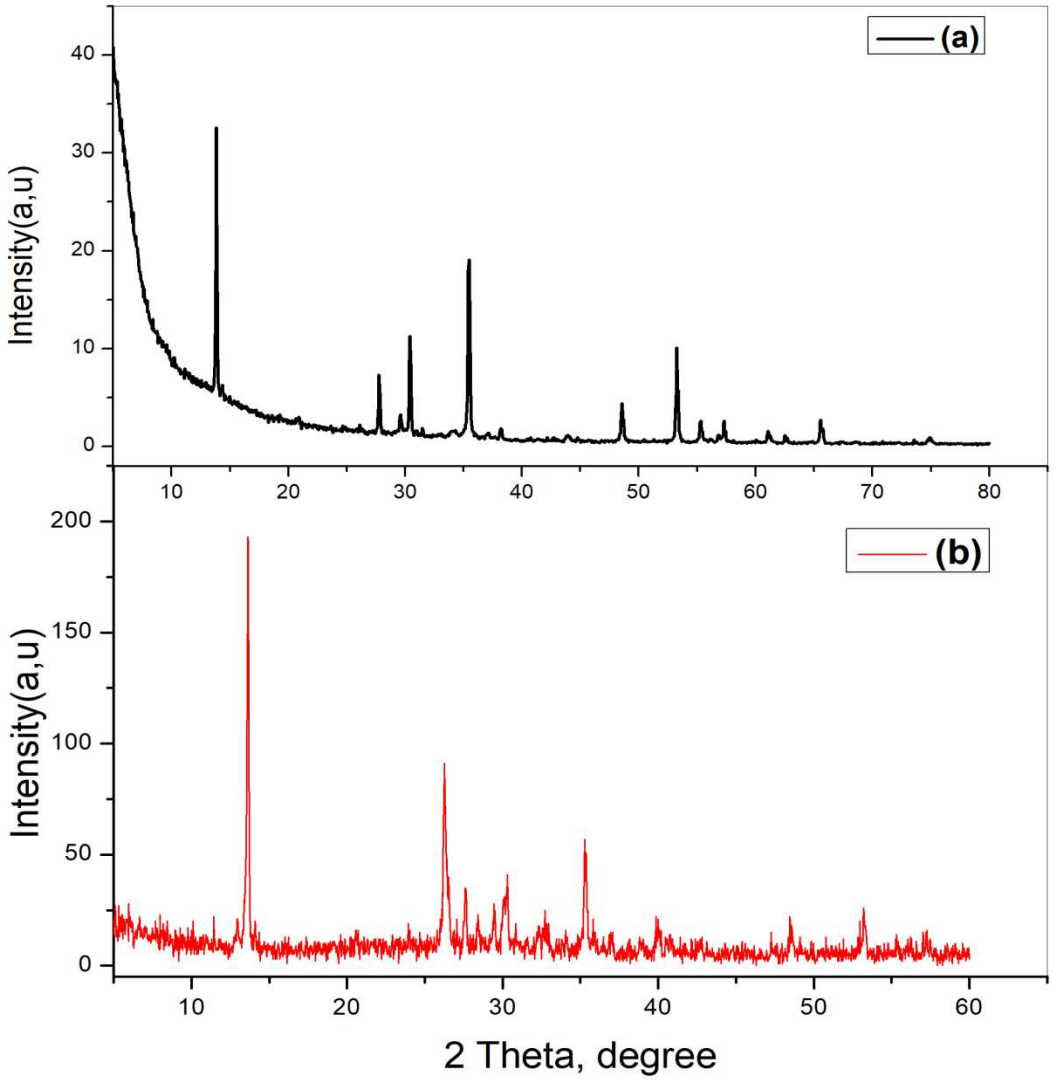



Figure 1: XRD of (a) $FePS_3$ and (b) $FePS_3$-CS

### 3.2. IR Measurement

The FTIR spectra of $FePS_3$ and the intercalated compound of $FePS_3$-CS are shown in Figure 2 (a, b). $FePS_3$ typically exhibited absorption bands associated with its bond. The presence of the strong stretching peak of $FePS_3$ at 570 $cm^{-1}$ has been observed, as shown in Figure 2(b)[29] . The vibrational stretching peaks around 500-600 $cm^{-1}$ corresponding to P-S. As shown in Figure 2(a), broad band of O-H and N-H stretching vibration around 3400 $cm^{-1}$, C-H band at 2900 $cm^{-1}$, C=O around 1630 $cm^{-1}$ and N-H at 1340 $cm^{-1}$. These

bands of CS confirm the successful partial intercalation or adsorption of CS into $FePS_3$ layers lead to hybrid composite enhancing adsorption properties.

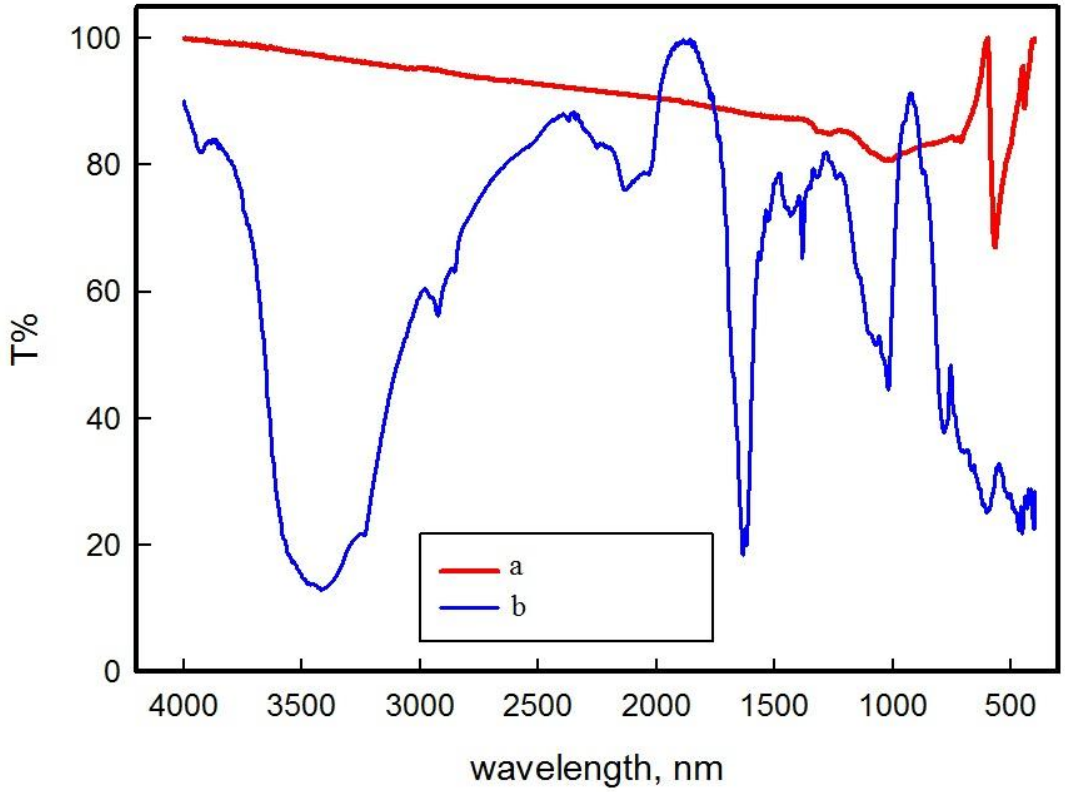



Figure 2: IR spectra of (a) $FePS_3$, and (b) $FePS_3$-CS.

### 3.3 SEM-EDX Measurement

Figure 3 (a, b) illustrates the SEM image of $FePS_3$ and $FePS_3$-CS, respectively. The pure $FePS_3$ sample shows a separate layered morphology as plates, reflecting lamellar crystalline structure[40]. The intercalation of CS changes the morphology of $FePS_3$. The regular layered structure becomes more fragmented and appearance of irregular particles. This confirms the successful intercalation or adsorption of CS within $FePS_3$. Moreover, the surface becomes porous which may increase the surface area and provide additional adsorption active sites for Congo-Red adsorption.

Figure 3 (c, d) presents the EDX spectra $FePS_3$ and $FePS_3$-CS. Respectively. The EDX spectrum of pure $FePS_3$ shows the peaks of Fe, P, and S without any impurities

signal[41]. The elemental wt. % were 33.13 Fe, 20.7 % P, and 46.17 % S, in good agreement with theoretical composition. These confirm the successful synthesis and high purity of $FePS_3$.

However, The EDX spectrum of $FePS_3$-CS displayed additional peaks for C and O elements. The composite contained 25.39 % Fe, 10.54 % P, 24.83 %S, 25.99 % C, and 13.25% O, carbon from polymeric structure of CS and oxygen from functional group of CS. The Fe, P, and S percentage intercalated sample lower than pure one, this indicates effectively modified by chitosan.

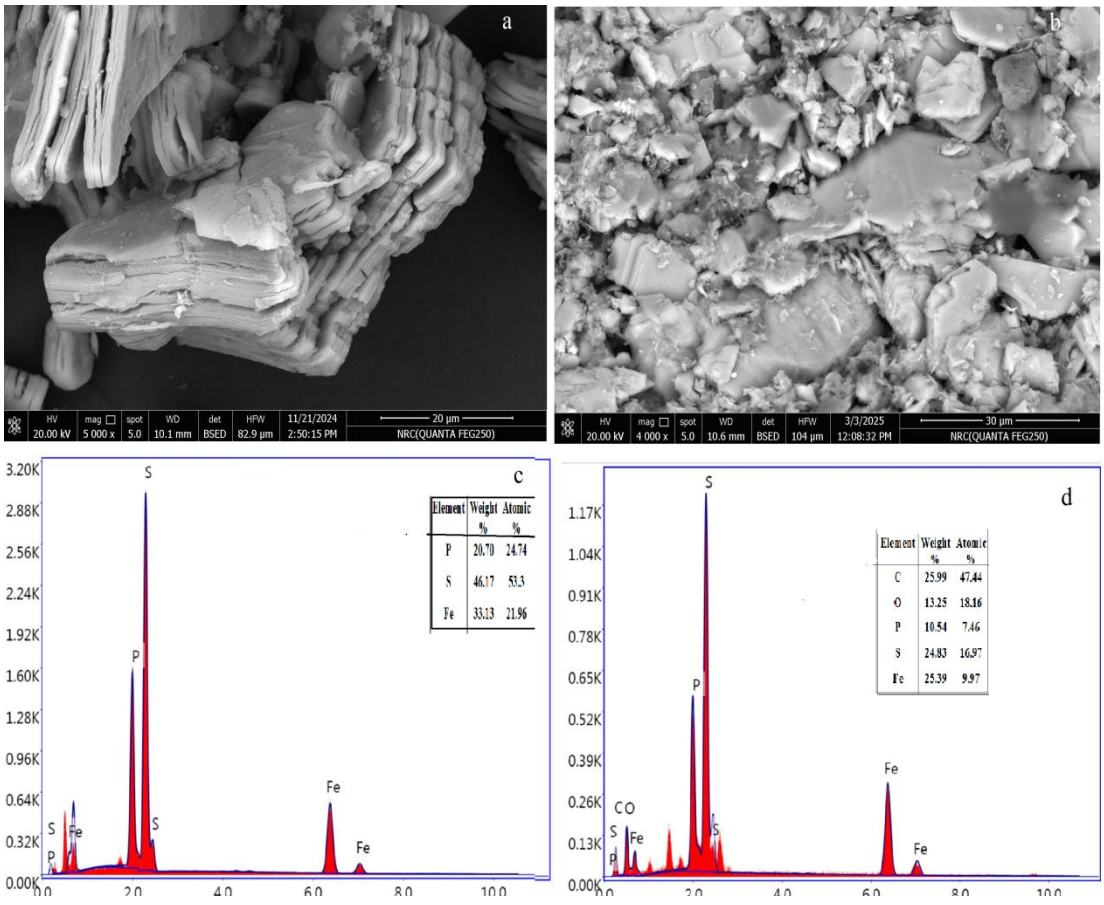



Figure 3: SEM images of (a) $FePS_3$ and (b) $FePS_3$-CS, and EDX graphs of (c) $FePS_3$ and (d) $FePS_3$-CS.

### 3.4. Surface area and porosity analysis

Nitrogen adsorption–desorption analysis was used to assess the prepared sample's textural characteristics. Figure 4 (a, b) shows the $N_2$ adsorption-desorption isotherms for pure $FeSP_3$ and $FeSP_3$-CS, respectively, providing crucial information about their porosity and surface area. In the (a) and (b) panels, the observed isotherm shows typical type II behavior together with a noticeable hysteresis loop, confirming the material's mesoporous nature , featuring an insignificant hysteresis loop at high relative pressures ($P/P^0$) more than 0.8 (Figure 4a).

This behavior suggests that the pure $FePS_3$ sample is mainly mesopores, where unlimited monolayer-multilayer adsorption on the exterior particle surfaces is the primary physisorption. Similarly, the $FeSP_3$-CS composite exhibits Type II isotherms with a comparable hysteresis loop, highlighting its mesopores character (Figure 4b). In contrast to the pure sample, a notable decrease in the maximum adsorption capacity at saturation pressure was observed. This reduction is attributed to the incorporation of chitosan particles on to the lattice structure of $FePS_3$.

The pore size distributions for pure $FeSP_3$ and $FeSP_3$-CS using the NLDFT model are represented in Figs. 4 (c, d). These distributions reveal information on the distribution of pore sizes in the materials. The distribution profile of the pure $FeSP_3$ sample is very uniform, with a sharp, unique peak that is perfectly centered at a pore width 4.72 nm. The cumulative total pore volume (Vp) computed using the NLDFT framework was determined to be $4.85 \times 10^{-2}$ $cm^3/g$ and an average pore diameter of 83.49 nm. These data demonstrate that the material is primarily microporous with poor surface development, which can be attributed to pore enlargement and partial disintegration of smaller pores during high-temperature. The specific surface area of pure FeSP3 is equal to 20.32 $m^2/g$. On the other hand, the pore size distribution of pure $FePS_3$ and $FeSP_3$-CS exhibiting a definite, sharp peak at a pore width at about 4.5 nm and about 26.38 nm, respectively, as shown in Figure 4 (c, d). The total pore volume increased significantly from $4.85 \times 10^{-2}$ $cm^3/g$ to 2.23 $cm^3/g$, while the average pore diameter dropped significantly from 83.49 nm to 35.7 nm. These findings are further supported by the NLDFT pore size distribution

research, showing a shift toward smaller pore sizes within the mesoporous range along with a broader distribution, indicating a more heterogeneous pore structure after modification.

In general, the $FeSP_3$/chitosan alteration results in a transformation from a predominantly microporous structure to a more developed mesoporous–microporous system, with better surface properties and pore accessibility. It is anticipated that these modifications will greatly increase adsorption performance, by making more active sites available and promoting mass transfer inside the porous network [42]. The BET surface area of $FeSP_3$-CS slightly increased to 50.49 $m^2/g$ compared to 20.32 $m^2/g$ for the pure sample

This variation in textural characteristics can be attributed to the incorporation and intercalation between chitosan and iron species. The chitosan matrix likely contributes to partial plug massive micropores decreasing the pore diameter while adding more functional groups that improve surface heterogeneity at the same time. Additionally, the interaction between iron species and the carbon framework may enhance pore connectivity and encourage the creation of new pores [43].

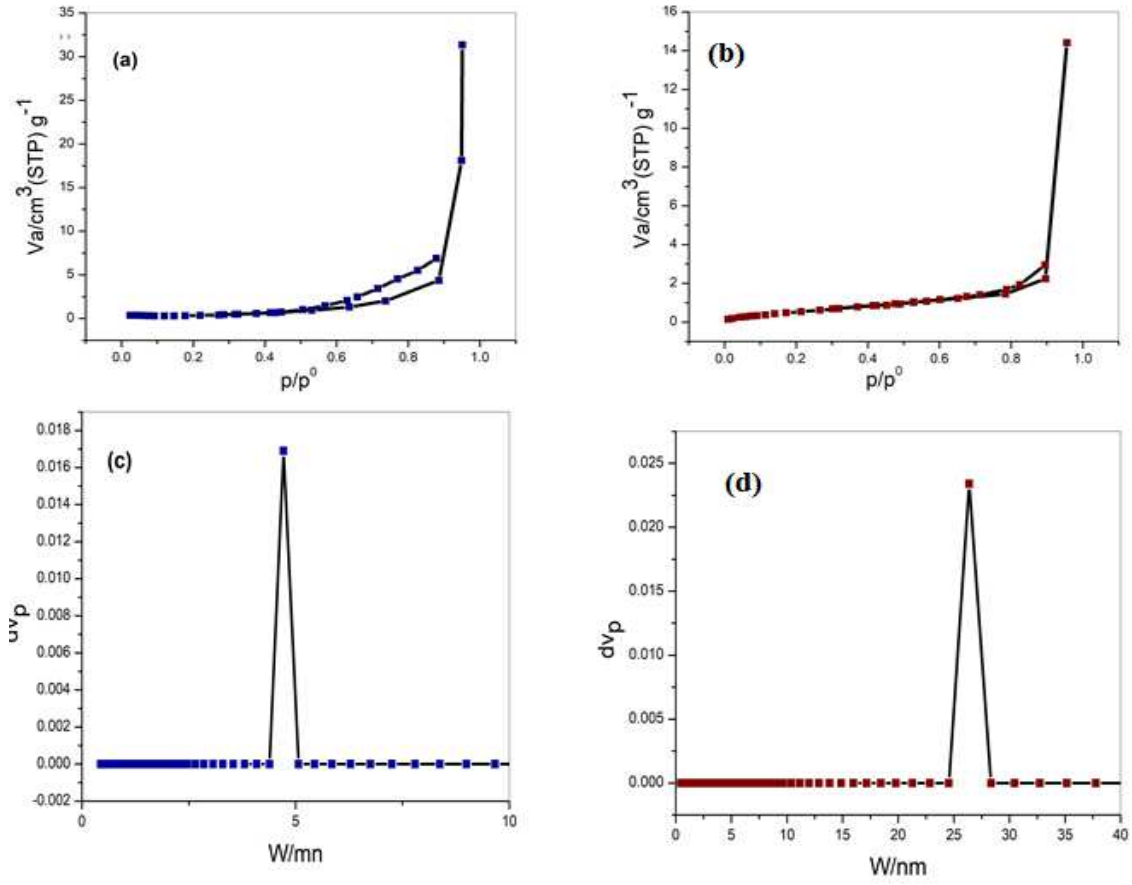



Figure 4: The $N_2$ adsorption-desorption isotherms for (a) $FeSP_3$ and (b) $FeSP_3$-CS combined by pore size distribution utilizing NLDFT model for (c) $FeSP_3$ and (d) $FeSP_3$-CS.

### 3.5. Adsorption Studies of $FePS_3$ and $FePS_3$- CS

#### *3.5.1. Effect of contact time on the CR dye adsorption*

In the adsorption tests, solutions containing 0.025 g of the $FePS_3$ and $FePS_3$–Chitosan and an initial dye concentration of 25 mg/L were combined and continuously swirled for periods varying from 15 to 120 minutes, while keeping other operational parameters constant. Figure 5 displays the impact of contact time on the effectiveness of Congo red dye removal using $FePS_3$and $FePS_3$–Chitosan. In light of the results [44] as the contact

time increased, the removal % for both adsorbents increased steadily until equilibrium was attained. The removal of $FePS_3$ began at roughly 73% after 10 minutes and rose gradually over time, reaching almost 91, 4 % at 90 minutes. No discernible improvement was seen after that, suggesting that the adsorption process had reached equilibrium. On the other hand, $FePS_3$–Chitosan showed significantly greater removal efficiency right away, removing 87% of the material after just 10 minutes. The adsorption kept growing quickly, reaching virtually total elimination (99%) at 90 minutes, and then staying practically constant.

Chitosan functional groups (-$NH_2$ and -OH) are responsible for $FePS_3$–Chitosan's better performance because they offer more active sites and improve the interaction between the adsorbent surface and Congo Red dye molecules . Comparing this to $FePS_3$ alone, the maximum removal efficiency is increased and the adsorption rate is accelerated [45] .

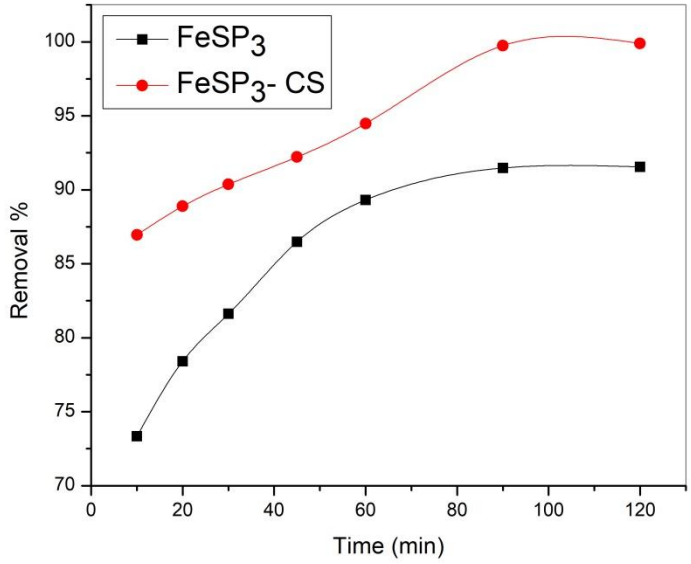



Figure 5: Effect of contact time on the removal of Congo red dye using $FePS_3$ and $FePS_3$–CS Adsorption conditions: dye concentration: 25 mg $L^{-1}$, adsorbent dose: 0.025 g, at room temperature

### *3.5.2. Effect of pH on the CR dye adsorption*

The impact of solution pH on Congo Red removal efficiency by $FePS_3$ and $FePS_3$-CS examined over the 2–9 range under controlled conditions: 0.025 g of the $FePS_3$ and $FePS_3$–CS an initial Congo-Red dye concentration (Co) of 25 mg/L, and for a 90-minute contact period, as shown in Figure (6). It was discovered that pH was a critical factor in the adsorption process for both adsorbents. By increasing the pH, the removal percentage of $FePS_3$ increased from 64% at pH 2 to a maximum to about 79% at pH 5. However, the efficiency fell precipitously with subsequent pH levels, peaking at 27% at pH 9. Based on this pattern, it appears that acidic conditions are optimal for $FePS_3$, since surface protonation increases the electrostatic attraction to the negatively charged Congo-Red molecules. The removal effectiveness decreases as the pH rises because surface functional group deprotonation results in negative charges and electrostatic repulsion with the anionic dye.

The removal effectiveness of $FePS_3$–CS was consistently higher than that of $FePS_3$ alone over the whole pH range. At pH 6, the highest adsorption (~97%) was achieved, which was marginally greater than $FePS_3$ [46] . Even at pH 9, the efficiency was above 80%. The presence of chitosan functional groups ($-NH_2$ and -OH) is responsible for this better performance. These groups offer extra active sites and can interact with Congo Red through hydrogen bonding, complexation, and electrostatic interactions. Protonated chitosan amino groups ($-NH_3^+$) increase electrostatic attraction with the anionic dye at acidic pH values, whereas near-neutral pH values preserve strong adsorption by supporting extra hydrogen-bonding interactions. In comparison to $FePS_3$ alone, $FePS_3$-CS exhibits greater maximum removal and wider pH stability overall, indicating the advantageous contribution of chitosan to enhancing the composite's adsorption capabilities [45, 47]

.

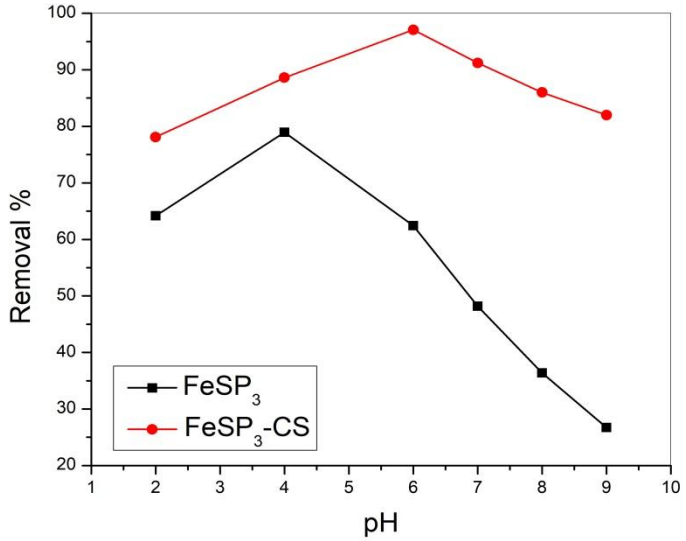



Figure 6: Effect of pH value of dye removal by pure $FePS_3$, $FePS_3$- chitosan (Adsorption conditions: dye concentration: 25 mg $L^{-1}$, adsorbent dose: 0.025 g, mixing time: 90 min and pH 2–9, at room temperature).

### *3.5.3. Effect of dose on the CR dye adsorption*

For both $FePS_3$ and $FePS_3$–Chitosan, the effect of adsorbent dose on the removal of Congo red dye was investigated in the range of 0.025–0.10 g, under controlled conditions: an initial Cong-Red dye concentration of 25 mg/L, pH maintained at 4, 6 for pure $FePS_3$, $FePS_3$-CS respectively and solution volumes set at 25 mL, at 90 minutes, as shown in Figure 7. The removal percentage for $FePS_3$ rose as the adsorbent dose increased, from approximately 59 % at 0.025 g to approximately 86% at 0.05 g, after which it stayed almost constant." This pattern is explained by the fact that active sites become more readily available as dose increases up until surface saturation, after which no improvement is possible. Conversely, $FePS_3$-CS displayed the reverse pattern. Although the removal was substantial (~81%) at 0.025 g, it decreased gradually with increase the dose, reaching about 40% at 0.10 g. This reduction could be the consequence of desorption effects at greater concentrations as well as particle aggregation and site overlap, which lower the effective surface area

According to these findings, $FePS_3$ functions normally, with greater dosages improving dye removal up until equilibrium is achieved. $FePS_3$-CS, on the other hand, works best at low doses and becomes less effective as dosage increases. Smaller doses of $FePS_3$-CS are more successful at removing Congo-Red; therefore, this odd tendency emphasizes the necessity for careful dose optimization [48, 49] .

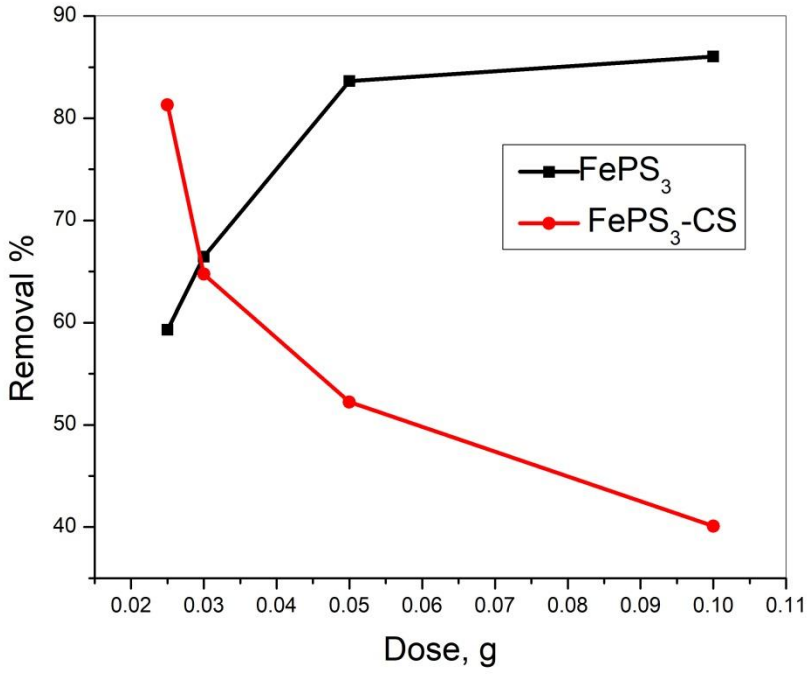



Figure 7: Effect of dose pure $FePS_3$, $FePS_3$-CS on Congo red dye removal (Adsorption conditions: dye concentration: 25 mg $L^{-1}$, mixing time: 90 min and pH= 4 for pure $FePS_3$, and pH=6 for $FePS_3$-CS, at room temperature).

### *3.5.4 Effect of dye concentration on the CR dye adsorption*

Figures 8 (a, b) illustrates the adsorption behavior of Congo red at various initial concentrations (5-50 mg/l) under controlled conditions: pH maintained at 4, 6 for pure $FePS_3$, $FePS_3$-CS respectively and solution volumes set at 25 mL, and 0.05g, 0.025 g for pure $FePS_3$, $FePS_3$-CS respectively at 90 minutes. The removal % is comparatively high at lower concentrations because the majority of dye molecules may readily access the active sites that are present.

Both $q_e$ (mg/g) and removal percentage increase with increasing initial concentration because the higher driving force promotes faster dye molecule diffusion onto the adsorbent surface. But beyond specific concentration, $q_e$ keeps rising while the removal percentage tends to level off.

This behavior is explained by the saturation of accessible sites: the percentage of dye removed in relation to the initial amount falls even though more dye is taken up per unit mass (higher $q_e$).

Furthermore, $FePS_3$–CS continuously exhibits higher $q_e$ and removal % as compared to $FePS_3$, demonstrating that the chitosan alteration improves adsorption efficiency and capacity.

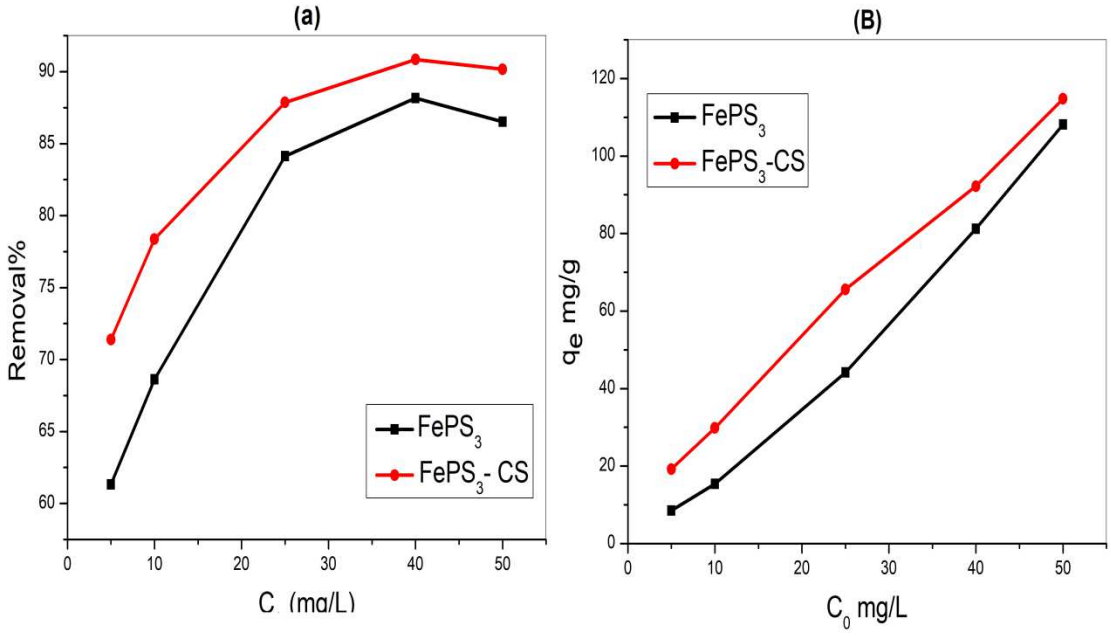



Figure 8: The effect of initial dye concentration (5-50 mg/l) by $FeSP_3$and $FeSP_3$-CS on: (a) CR removal rate and (b) the amount of CR adsorbed at equilibrium.

### *3.5.4. Isotherms of adsorption*

Langmuir, Freundlich, and Temkin isotherm models were used to analyse the equilibrium data in order to gain insight into the adsorption mechanism of Congo-Red dye (Table 1).

With $FePS_3$, a maximum monolayer adsorption capacity ($Q_m$) of 102.24 mg/g with a correlation coefficient ($R^2$) of 0.933 was predicted using the Langmuir model. The comparatively high $Q_m$ value suggests that there are a significant number of active sites in $FePS_3$ that are accessible to dye uptake. On the other hand, the Freundlich model provided an even better correlation ($R^2$ = 0.974), with 1/n = 0.7939 and a Freundlich constant KF of 1.842.

This implies that Congo red adsorption on $FePS_3$takes place on a heterogeneous surface, involving multilayer adsorption and varied energy sites, as 1/n values between 0 and 1 indicate favorable adsorption. This suggests that surface heterogeneity cannot be disregarded for $FePS_3$, even though monolayer adsorption is feasible. The Langmuir model also predicted a greater maximum adsorption capacity ($Q_m$ = 113.12 mg/g) and suitable well for $FePS_3$-CS ($R^2$ = 0.979), demonstrating the positive impact of chitosan in improving the adsorption performance.

Although both processes are spontaneous, $FePS_3$ has a slightly stronger binding affinity than $FePS_3$-CS, which has a larger overall capacity, as indicated by the more negative $\Delta G°$ value found for $FeSP_3$ (−32.64 kJ/mol) as opposed to $FePS_3$–Chitosan (−24.12 kJ/mol).

Remarkably, with KF = 3.70 and 1/n = 0.4086, the Freundlich model provided the strongest correlation for $FePS_3$-CS ($R^2$ = 0.997). A more favorable adsorption process is shown by the significantly lower 1/n value, which implies that chitosan provides stronger surface heterogeneity and a larger distribution of binding sites. This lends evidence to the idea that $FeSP_3$-CS adsorbs dye molecules by a variety of processes, including as surface complexation, hydrogen bonding, and electrostatic attraction.

For both samples, the Temkin model revealed a weaker correlation, indicating that multilayer adsorption and surface heterogeneity are the main processes.

Overall, chitosan improved surface heterogeneity and adsorption capacity, increasing the removal efficiency of $FePS_3$-CS for Congo-Red.

Table (1) Langmuir, Freundlish and Temkin isotherms for CR dye adsorption.

| Model | Parameters | $FePS_3$ | $FePS_3$-CS |
|---|---|---|---|
| Langmuir isotherm | $Q_m$(mg/g) | 102.240 | 113.120 |
| | $K_L$(mg/L) | 0.758 | 0.024 |
| | $R^2$ | 0.933 | 0.979 |
| | $\Delta G^o$ (kJ/mol) | -32.640 | -24.127 |
| Freundlish isotherm | $K_F$(mg/g (l/mg)$^{1/n}$) | 1.842 | 3.70 |
| | 1/n | 0.794 | 0.409 |
| | $R^2$ | 0.974 | 0.997 |
| Temkin isotherm | B (kJ/mol) | 88.108 | 90.32 |
| | KT (L/g) | 0.380 | 0.937 |
| | $R^2$ | 0.882 | 0.913 |

### 3.6 Kinetics of adsorption

The pseudo-first-order, pseudo-second-order, and intraparticle diffusion models were used to assess adsorption kinetics (Table 2). With high $R^2$ values (0.9982 and 0.9997, respectively) and computed $q_e$ values that were in close agreement with the experimental data, the pseudo-second-order model offered the best fit for both $FePS_3$ and $FePS_3$–CS. This suggests that chemisorption involving electron sharing or exchange mostly controls adsorption. Diffusion is not the only rate-controlling step, as the intercept ($C \neq 0$) in the intraparticle diffusion plots indicates, but it does contribute to the adsorption process. According to the data, Congo-Red adsorption on $FePS_3$ and $FePS_3$–CS is primarily accomplished by chemisorption.

Table 3 shows the comparison of maximum efficiency for dye adsorption by different crosslinked CS adsorbents for Congo-Red dye removal. As is noticed, pure $FePS_3$ and $FePS_3$-CS composite show high efficiency of Congo-Red removal.

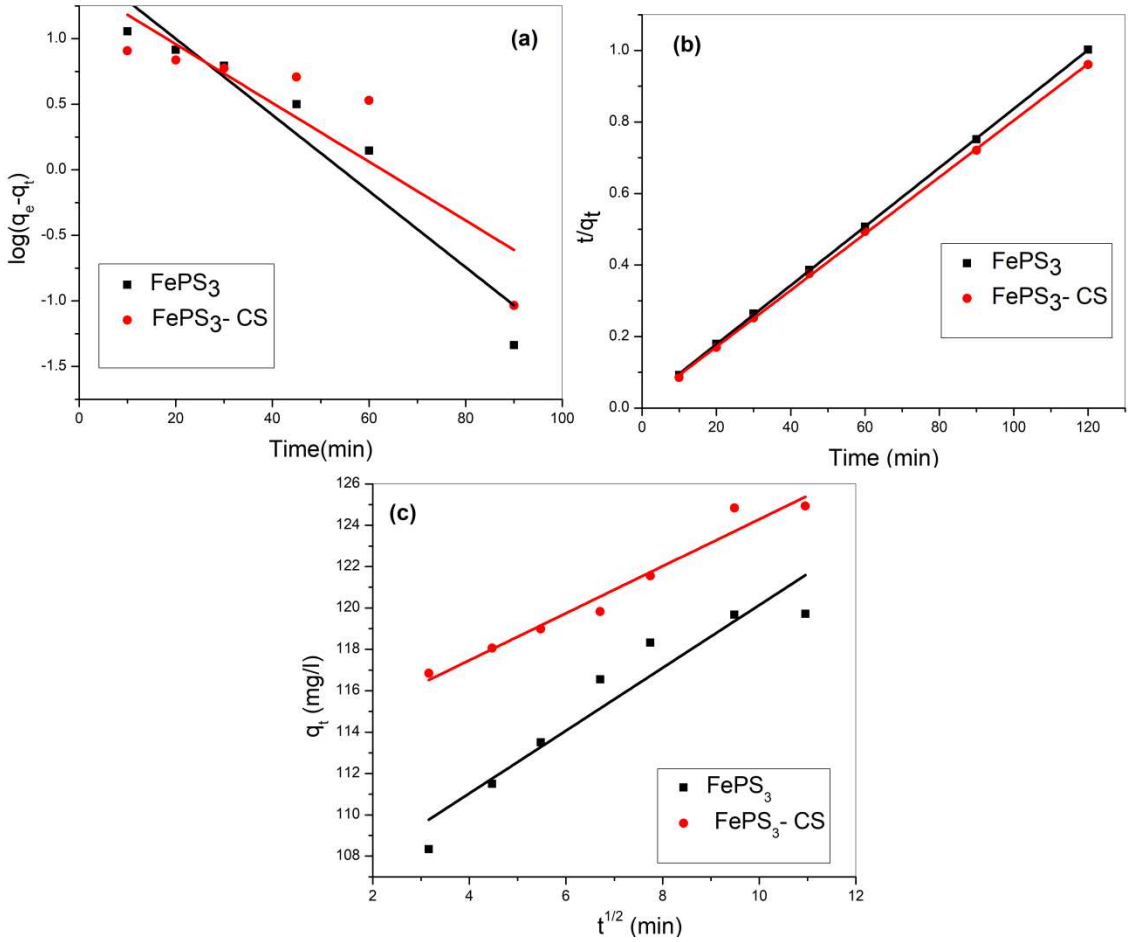



Figure 9: Plots of (a) pseudo-first order kinetic (b) pseudo-second order kinetic and (c) Intraparticle diffusion models

Table (2) Adsorption kinetic constants calculated for adsorption of CR dye over $FePS_3$ and $FePS_3$-CS $_3$samples.

| Model | parameters | $FePS_3$ | $FePS_3$- CS |
|---|---|---|---|
| Pseudo-first-order | $q_e$, exp (mg/g) | 119.7 | 124.9 |
| | $q_e$,cal (mg/g) | 38.01 | 29.24 |
| | $k_1$ ($min^{-1}$) | 0.0668 | 0.0557 |
| | $R^2$ | 0.90206 | 0.7325 |
| Pseudo-second-order | $q_e$, cal (mg/g) | 121.5 | 126.4 |
| | $k_2$ (g/mg.min) | $4.876*10^{-3}$ | $4.842*10^{-3}$ |
| | $R^2$ | 0.9982 | 0.9997 |
| Intraparticle diffusion | kd (mg/g min1/2) | 1.5159 | 1.13695 |
| | C | 104.977 | 112.922 |
| | $R^2$ | 0.89309 | 0.9574 |

Table (3) Comparison of the maximum Efficiency for dyes adsorption by different crosslinked CS adsorbents for Congo-Red dye removal.

| **Adsorbent** | **Removal %** | **Ref** |
|---|---|---|
| Trimesoyl chloride crosslinked chitosan | 99.4 | [48] |
| Chitosan-BN-$Fe_2O_3$ | 99.58 | [50] |
| Ni*0.5*Mn0.5$Fe_2O_4$/CS | 74 | [51] |
| Hydrogels Based on Chitosan, Acrylamide and Graphene Oxide | 85 | [52] |
| nano-chitosan | 99.69 | [53] |
| Glutaraldehyde-crosslinked CS | 87 | [54] |
| $FePS_3$ | 91.4 | Present |
| $FePS_3$-CS | 99 | work |

### 3.8. Reusability

For practical applications, adsorbents need to be reusable and regenerable to some extent. To assess the regeneration performance of the $FePS_3$ and intercalated $FePS_3$-CS, we estimated adsorption–desorption cycle trials. 0.1 mol/L HCl solution was used as a more effective eluting agent for six desorption investigations. For $FePS_3$ and $FePS_3$-CS, the removal efficiency decreased from 91.4 to 40% and 99 to 50% after six cycles, respectively, Fig(10). In conclusion, it is clear that the $FePS_3$ and $FePS_3$-CS can be recycled and used as a useful adsorbent to get rid of organic dyes.

An overview of different crosslinked CS adsorbents for Congo-Red dye removal is shown in Table 3. These results imply that $FePS_3$ and $FePS_3$-CS are a promising material for congo dye absorption due to its higher adsorption capacity when compared to other adsorbents.

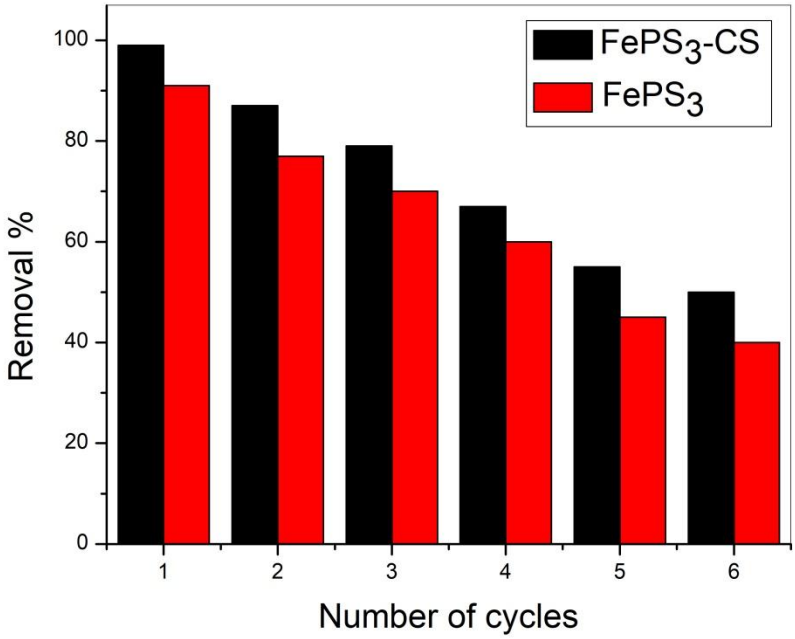



**Figure. 10** Removal efficiency of congo red by $FePS_3$ and $FePS_3$-CS after 6 cycles

## 4. Conclusion

Black powder of $FePS_3$ was prepared after mixing stoichiometric amounts of pure elements (about 99.9% purity of Fe, P, and S)) and the mixture was put in a silica tube. Sealing of the silica tube was processed under vacuum, and the sealed tube was placed in a programmed furnace to run the solid-state reaction at 650 $^{o}$C for 3 days. The novel intercalation of the CS into the layered material FePS3 was operated using wet-chemical method by stirring for 10 hrs at 60 $^{o}$C. The XRD result shows slight shift of hkl phase of FePS3. The results of surface area and porosity analysis show a transformation from a predominantly macroporous structure of pure $FePS_3$ to a more developed mesoporous–macroporous of $FePS_3$-CS intercalated compound, with better surface properties and pore accessibility. The adsorption kinetics of Congo-Red removal indicates that it follows chemisorption mechanism. The removal of CR by $FePS_3$ began at roughly 73% after 10 minutes and rose gradually over time, reaching almost 91.4 % at 90 minutes. No discernible improvement was seen after that, suggesting that the adsorption process had

reached equilibrium. On the other hand, $FePS_3$–CS showed significantly greater removal efficiency right away, removing 87% of the material after just 10 minutes. The adsorption kept growing quickly, reaching virtually total elimination (~99%) at 90 minutes, and then staying practically constant.

**Statements and Declarations:**

**Competing interests:** We confirm that there is no conflict of interest.

**Data availability:** The datasets used and/or analyzed during the current study are available from the authors on request.

**Supplementary information:** There is no any additional material.

**Ethical approval:** No applicable.

**Funding**: No funding

**References**

[1] P.O. Ukaogo, U. Ewuzie, C.V. Onwuka, Environmental pollution: causes, effects, and the remedies, in: Microorganisms for sustainable environment and health, Elsevier, 2020, pp. 419-429.
[2] S.S. Shetty, D. Deepthi, S. Harshitha, S. Sonkusare, P.B. Naik, H. Madhyastha, Environmental pollutants and their effects on human health, Heliyon, 9 (2023).
[3] R.R. Appannagari, Environmental pollution causes and consequences: a study, North Asian International Research Journal of Social Science & Humanities, 3 (2017) 151-161.
[4] X. Qin, H. Cui, Q. Zhou, Physisorption behaviors of organochlorine pesticides on the InP3 monolayer from theoretical insight, ACS omega, 8 (2023) 32168-32175.
[5] H.B. Slama, A. Chenari Bouket, Z. Pourhassan, F.N. Alenezi, A. Silini, H. Cherif-Silini, T. Oszako, L. Luptakova, P. Golińska, L. Belbahri, Diversity of synthetic dyes from textile industries, discharge impacts and treatment methods, Applied Sciences, 11 (2021) 6255.

[6] D. Bhatia, N.R. Sharma, J. Singh, R.S. Kanwar, Biological methods for textile dye removal from wastewater: A review, Critical Reviews in Environmental Science and Technology, 47 (2017) 1836-1876.
[7] R. Jamee, R. Siddique, Biodegradation of synthetic dyes of textile effluent by microorganisms: an environmentally and economically sustainable approach, European journal of microbiology and immunology, 9 (2019) 114-118.
[8] H.A. Saleh, S.E. El-Shafey, A.M. Abdel-karim, M.S. Tohamy, A.A. El-Meligi, Investigating magnetic and optical properties of layered iron phosphorus trisulfide intercalated with organic compounds, Physica Scripta, 100 (2025) 025522.
[9] A.A. El-Meligi, A.M. Abdel-karim, A.A. Abbas, Intercalation of layered nanomaterial with organic compounds and effect on magnetic properties, Chemistry Africa, 7 (2024) 2693-2701.
[10] I. Cabria, A. El-Meligi, DFT simulation of hydrogen storage on manganese phosphorous trisulphide (MnPS3), International Journal of Hydrogen Energy, 43 (2018) 5903-5912.
[11] N. Ismail, A. El-Meligi, Y. Temerk, M. Madian, Synthesis and characterization of layered FePS3 for hydrogen uptake, international journal of hydrogen energy, 35 (2010) 7827-7834.
[12] J.-U. Lee, S. Lee, J.H. Ryoo, S. Kang, T.Y. Kim, P. Kim, C.-H. Park, J.-G. Park, H. Cheong, Ising-type magnetic ordering in atomically thin FePS3, Nano letters, 16 (2016) 7433-7438.
[13] M. Amirabbasi, P. Kratzer, Orbital and magnetic ordering in single-layer FePS 3: A DFT+ U study, Physical Review B, 107 (2023) 024401.
[14] M.L.A.U. Liyanage, Synthesis of Intercalation Compounds and Nanocomposites of Inorganic Layered Hosts, (2015).
[15] A.A. El-Meligi, E.H. Ahmed, A.M. Abdel-Karim, A.A. Abbas, B.S. Nabawy, Investigating magnetic and optical properties and morphology of a nanocomposite of intercalated layered material and polymer compounds, Scientific Reports, 16 (2026) 15486.
[16] A.A. El-Meligi, T.A. Farghaly, A.M. Alsaedi, A.M. Abdel-karim, Investigating Changes in the Magnetic and Optical Properties of FePS3 upon Intercalation with bis-spiropyrazole, Journal of Molecular Structure, (2025) 144121.
[17] F. Wang, T.A. Shifa, P. Yu, P. He, Y. Liu, F. Wang, Z. Wang, X. Zhan, X. Lou, F. Xia, New frontiers on van der Waals layered metal phosphorous trichalcogenides, Advanced Functional Materials, 28 (2018) 1802151.
[18] H. Zhang, T. Wei, Y. Qiu, S. Zhang, Q. Liu, G. Hu, J. Luo, X. Liu, Recent progress in metal phosphorous chalcogenides: potential high-performance electrocatalysts, Small, 19 (2023) 2207249.
[19] M. Rinaudo, Chitin and chitosan: Properties and applications, Progress in polymer science, 31 (2006) 603-632.

[20] A. Pellis, G.M. Guebitz, G.S. Nyanhongo, Chitosan: sources, processing and modification techniques, Gels, 8 (2022) 393.
[21] J. Huang, Z. Zong, P. Wang, Y. Zhang, D. Gao, Y. Wang, Z. Li, Machine learning-driven simulation and optimization of phosphate adsorption on metal-organic frameworks, Separation and Purification Technology, (2026) 137479.
[22] V.K. Gupta, Application of low-cost adsorbents for dye removal–a review, Journal of environmental management, 90 (2009) 2313-2342.
[23] A. Islam, S.H. Teo, Y.H. Taufiq-Yap, C.H. Ng, D.-V.N. Vo, M.L. Ibrahim, M.M. Hasan, M.A.R. Khan, A.S. Nur, M.R. Awual, Step towards the sustainable toxic dyes removal and recycling from aqueous solution-A comprehensive review, Resources, Conservation and Recycling, 175 (2021) 105849.
[24] S. Rosa, M.C. Laranjeira, H.G. Riela, V.T. Fávere, Cross-linked quaternary chitosan as an adsorbent for the removal of the reactive dye from aqueous solutions, Journal of hazardous materials, 155 (2008) 253-260.
[25] N. Tara, S.I. Siddiqui, G. Rathi, S.A. Chaudhry, Inamuddin, A.M. Asiri, Nano-engineered adsorbent for the removal of dyes from water: A review, Current Analytical Chemistry, 16 (2020) 14-40.
[26] L.D. Ardila-Leal, R.A. Poutou-Piñales, A.M. Pedroza-Rodríguez, B.E. Quevedo-Hidalgo, A brief history of colour, the environmental impact of synthetic dyes and removal by using laccases, Molecules, 26 (2021) 3813.
[27] B. Sharma, S. Tiwari, R. Kumar, M. Kumar, L. Tewari, Eco-friendly detoxification of hazardous Congo red dye using novel fungal strain Trametes flavida WTFP2: Deduced enzymatic biomineralization process through combinatorial in-silico and in-vitro studies, Journal of Hazardous Materials, 455 (2023) 131503.
[28] K.L. Maurya, G. Swain, R.K. Sonwani, A. Verma, R.S. Singh, Biodegradation of Congo red dye using polyurethane foam-based biocarrier combined with activated carbon and sodium alginate: Batch and continuous study, Bioresource technology, 351 (2022) 126999.
[29] A. El-Meligi, Synthesizing layered material of FePS3 and its intercalation with pyridinum, Materials chemistry and physics, 89 (2005) 253-259.
[30] Y.-S. Ho, G. McKay, Sorption of dye from aqueous solution by peat, Chemical engineering journal, 70 (1998) 115-124.
[31] S. Lagergren, Zur theorie der sogenannten adsorption geloster stoffe, (1898).
[32] W.J. Weber Jr, J.C. Morris, Kinetics of adsorption on carbon from solution, Journal of the sanitary engineering division, 89 (1963) 31-59.
[33] I. Langmuir, The adsorption of gases on plane surfaces of glass, mica and platinum, Journal of the American Chemical society, 40 (1918) 1361-1403.
[34] H.M.F. Freundlich, Over the adsorption in solution, J. Phys. chem, 57 (1906) 1100-1107.

[35] R. Basnet, K.M. Kotur, M. Rybak, C. Stephenson, S. Bishop, C. Autieri, M. Birowska, J. Hu, Controlling magnetic exchange and anisotropy by nonmagnetic ligand substitution in layered MPX 3 (M= Ni, Mn; X= S, Se), Physical Review Research, 4 (2022) 023256.
[36] G. Long, T. Zhang, X. Cai, J. Hu, C.-w. Cho, S. Xu, J. Shen, Z. Wu, T. Han, J. Lin, Isolation and characterization of few-layer manganese thiophosphite, ACS nano, 11 (2017) 11330-11336.
[37] Y. Shemerliuk, Y. Zhou, Z. Yang, G. Cao, A.U. Wolter, B. Büchner, S. Aswartham, Tuning magnetic and transport properties in quasi-2D (Mn1− xNix) 2P2S6 single crystals, Electronic Materials, 2 (2021) 284-298.
[38] A. El-Meligi, Investigation of MnPS3 intercalates with pyridinium ion, Materials chemistry and physics, 84 (2004) 331-340.
[39] M. Kong, X.G. Chen, K. Xing, H.J. Park, Antimicrobial properties of chitosan and mode of action: a state of the art review, International journal of food microbiology, 144 (2010) 51-63.
[40] Y. Ding, Y. Chen, N. Xu, X. Lian, L. Li, Y. Hu, S. Peng, Facile synthesis of FePS3 nanosheets@ MXene composite as a high-performance anode material for sodium storage, Nano-micro letters, 12 (2020) 54.
[41] N.M. Latiff, C.C. Mayorga-Martinez, B. Khezri, K. Szokolova, Z. Sofer, A.C. Fisher, M. Pumera, Cytotoxicity of layered metal phosphorus chalcogenides (MPXY) nanoflakes; FePS3, CoPS3, NiPS3, FlatChem, 12 (2018) 1-9.
[42] X. Li, Y. Li, Y. Li, M. Zhang, J. Zhu, Synthesis of Lignin-Derived Hierarchical Porous Carbon via Hydrothermal–Phosphoric Acid Synergistic Activation for Enhanced Adsorption of Tetracycline, Molecules, 31 (2026) 447.
[43] N.A. Fathy, S. El-Shafey, Effect of Acid Soaking on Properties of Zeolite-Based Porous Carbon Composite Prepared for Adsorption of Cationic Dye, Chemistry Africa, 7 (2024) 1535-1545.
[44] M. Harja, G. Buema, D. Bucur, Recent advances in removal of Congo Red dye by adsorption using an industrial waste, Scientific Reports, 12 (2022) 6087.
[45] R. Lafi, I. Montasser, A. Hafiane, Adsorption of congo red dye from aqueous solutions by prepared activated carbon with oxygen-containing functional groups and its regeneration, Adsorption Science & Technology, 37 (2019) 160-181.
[46] S. Elhady, M. Bassyouni, M.Z. Elshikhiby, M.Y. Saleh, M.H. Elzahar, Advanced chitosan-based composites for sustainable removal of congo red from textile wastewater, Discover Sustainability, 5 (2024) 271.
[47] N. Fathy, S. El-Shafey, Carbon-based nanohybrid fabricated in-situ and boosted the adsorption of anionic reactive yellow dye, International Journal of Environmental Science and Technology, 20 (2023) 293-306.
[48] A.K. Shukla, J. Alam, M. Alhoshan, Trimesoyl chloride crosslinked chitosan: An efficient adsorbent for Congo red dye removal from water-kinetic and isotherm analysis, International Journal of Biological Macromolecules, 319 (2025) 145538.

[49] M.A. El-Kemary, I.M. El-mehasseb, K.R. Shoueir, S.E. El-Shafey, O.I. El-Shafey, H.A. Aljohani, R.R. Fouad, Sol-gel TiO2 decorated on eggshell nanocrystal as engineered adsorbents for removal of acid dye, Journal of Dispersion Science and Technology, 39 (2018) 911-921.
[50] M.S. Bingöl, Removal of Congo Red from water by adsorption onto Chitosan-BN-Fe2O3: Kinetic and isotherm studies, Erzincan University Journal of Science and Technology, 15 (2022) 684-698.
[51] N. Rasouli, H. Salavati, M. Movahedi, A. Rezaei, An Insight on kinetic adsorption of Congo red dye from aqueous solution using magnetic chitosan based composites as Adsorbent, Chem. Methodol, 1 (2017) 74-86.
[52] J. Amtul, N. Yasha, N. Sitara, Elimination of a carcinogenic anionic dye Congo red from water using hydrogels based on chitosan, acrylamide and graphene oxide, Journal of Bioprocessing & Biotechniques, 8 (2018) 2155-9821.
[53] H. Rezaei, A. Razavi, A. Shahbazi, Removal of Congo red from aqueous solutions using nano-Chitosan, Environmental Resources Research, 5 (2017) 25-34.
[54] N.S. Dissanayake, M.A. Pathirana, N.D. Wanasekara, B. Mahltig, G.K. Nandasiri, Removal of methylene blue and congo red using a chitosan–graphene oxide-electrosprayed functionalized polymeric nanofiber membrane, Nanomaterials, 13 (2023) 1350.